Membrane Technology
ISSN (online): 1873-4049

Laboratory Tests and Simulations on Loading Performance of Cold-Formed Steel Purlin-to-Sheet Roofing Structures

Ming Gao[1], Liming Ji[1], Fenghua Shi[1], Jiaqiang Sun[1], Zhirong Zheng[2], Feiliang Wang[3,4,*]

[1]*State grid Quzhou Power Supply Company, Quzhou 324022, China*

[2]*Quzhou Guangming Electric Power Design Co., LTD, Quzhou 324022, China*

[3]*Shanghai Key Laboratory for Digital Maintenance of Buildings and Infrastructure, School of Ocean and Civil Engineering, Shanghai Jiao Tong University, Shanghai 200240, China*

[4]*State Key Laboratory of Ocean Engineering, Shanghai Jiao Tong University, Shanghai 200240, China*

**Corresponding Author.*

Abstract:

Cold-formed steel (CFS) purlins, which possess a high load-carrying capacity compares to their weight, are extensively utilized in roof systems. Within purlin-to-sheet systems, roofing sheets provide additional lateral restraint to purlins, thereby enhancing the load-bearing capacity of the system. This research conducts both laboratory tests and simulations to evaluate the behavior of purlin-sheet systems under downward loading, focusing on ultimate bending moment and failure modes. To enhance predictive precision, a meticulous exploration of influential parameters is undertaken through comprehensive parametric analysis, identifying purlin thickness, steel material strength, roofing sheet thickness, and the number of lateral struts as critical factors influencing load-bearing capacity. It indicates that thickness, yield strength and lateral sturts of the purlins significantly impact structural load-bearing performance, whereas the contribution of roof panel thickness to load capacity is comparatively minor. For the purlin with small shell thickness (i.e., less than 1.5 mm), the main failure modes are distortional buckling at the upper flange and local buckling at the web. As the thickness of the purlin increases, the main buckling mode gradually shifts towards distortional buckling.

Keywords: purlin-sheet system, cold-formed steel, numerical simulation, load-carrying capacity, parametric analysis.

INTRODUCTION

Cold-formed steel (CFS) sections are prevalently employed as roof purlins or wall rails by virtue of their high-efficiency constructability. The steel sheet attached to the purlin flange offers lateral support to the purlin, thereby augmenting the structural stability. Normally, CFS purlins come in zed (Z), channel (C), and sigma (Σ) configurations, with the first two having a flat web and the latter possessing two indentations on the web. These sections are produced via press-breaking or cold-rolling from steel coils at room temperature and are typically pre-galvanized. Owing to their thin-walled characteristics and loading circumstances [1], CFS purlins, whether single span, overlapped [2] or continuous [3], are prone to local buckling (LB), distortional buckling (DB), and lateral-torsional buckling (LTB).

Purlins and sheets are instances of CFS applications and are often employed for roofing or wall cladding on the structural framework. The connection between the purlin and sheet is usually fastened by self-drilling screws. The design of purlins ought to take into account the contribution introduced by the sheet [4]. Zhang and Tong [5] disclosed the behaviour in lateral constrained purlins and proposed two theoretical models to explain the buckling of those components. The impact of lateral support on the instability of CFS purlins was investigated by Zhang and Tong [6] to assess the anti-sag bar's efficiency in delivering lateral restraint. Ye et al. [7,8] presented research on the failure behavior of CFS roof systems under uplift load scenario. Their analysis identified two types of restraints offered by the steel sheet, namely translational spring Ks and rotational spring Kr. The numerical analysis demonstrated that Ks having a greater influence on local buckling and Kr having a more significant effect on lateral-torsion buckling. Both springs have a combined influence in the distortional buckling mode.

Relevant specific design methods have been proposed in the European standard [9]. Nevertheless, the design methods in EN 1993-1-3 (EC3) standards have been criticized for the limitations of their parameters [10]. Zhao et al. examined the influence of screw spacing and load direction and suggested an analytical prediction method for rotational stiffness [11]. Soroushian and Peköz discovered that torsional deformation and vertical bending deformation are the main constituents of deformation in roof systems under wind loads [12]. Basaglia et al. [13] explored and analyzed the instability characteristics of CFS purlins supported by sheets under wind load. Georgescu and Ungureanu [14] performed a full-scale test on roof panels reinforced by purlins with overlapped segments at intermediate restraints. Gajdzicki [15] examined the rotational bracing effect provided by the sheet to the purlin, employing a configuration with two fasteners placed near the trapezoidal sheet webs in alternate troughs. The research highlighted that this setup could enhance the rotational stiffness and, consequently, improve the bending strength of cold-formed

Z-purlins. Kujawa and Szymczak [16] conducted a numerical evaluation of the rotational rigidity of zed-purlin connections to sandwich panels. Yang and Liu [17] carried out multiple investigations into the interaction between purlins and sheeting, showcasing the advantages of providing lateral or rotational bracing.

TESTS OF PURLIN-SHEET SYSTEM

A four-point loading experiment was carried out on four samples with diverse purlin cross-sections to determine their maximum bending moment capabilities. Each sample consisted of a couple of parallel 3-meter-long purlins placed with opposite surfaces and connected to concrete blocks by steel cleats that were held in place with M12 bolts (having a diameter of 12 mm). Trapezoidal sheets were fastened to purlins with screws positioned at each trough of the sheet and along the centerline of the flange of purlin. Steel beams with rectangular hollow sections (RHS) were used as load distributors on top of the attached sheets. The test incorporated four distinct Z-sections, namely Z14614, Z14618, Z20618, and Z30720, which are detailed in Table 1. Also, two bracing struts with C-sections (C49x20x12x0.8) were attached to the purlins using bolts and nuts (Figure 1b) to reduce LTB by supplying additional lateral supports. The sheet cross-section used in the test is illustrated in Figure 2.

Table 1. List of specimens

Specimen	Depth (mm)	Flange (mm)	Lips (mm)	Shell thickness (mm)
Z14614	145.0	62.5	20.0	1.4
Z14618	145.0	62.5	20.0	1.8
Z20618	200.0	65.0	20.0	1.8
Z30720	300.0	75.0	20.0	2.0

During the test, two LVDTs were vertically positioned on top of the secondary load distributor RHS, while the remaining two LVDTs were situated horizontally and vertically at the midpoint of the purlins' span. The placement locations of the LVDTs during testing are illustrated in Figure 3. Deflections measured by the LVDTs and data from the load cell were automatically recorded.

(a) Top view (b) Bottom view

Figure 1. Setup of four-point loading test

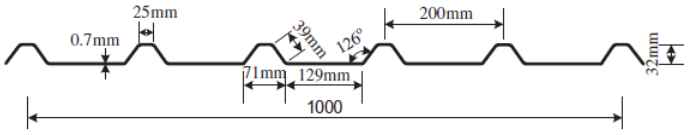

Figure 2. Section of the sheet adopted in the test

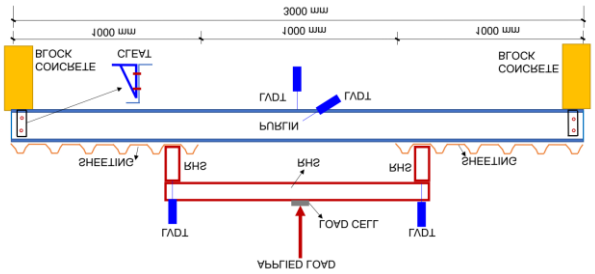

Figure 3. Measurement arrangement

NUMERICAL SIMULAITON METHOD

ABAQUS was applied to in the study to replicate the experimental arrangements. S4R element were utilized to model purlins and roof sheets, and R3D4 element were used to represent screws under the assumption that the screw stiffness was sufficient to avoid deformation. Material characteristics like elastic modulus and stress-strain curves (as depicted in Figure 4) were selected based on the coupon tests. In the numerical model, the material definitions were determined accrding to the coupon tensile test. "Tie" connections were established for the connections between screws and purlins and between purlins and struts. Bushing spring elements were used to represent the contact between screws and roof sheets to model the screw-hole interactions. To reduce penetration problems, a "hard contact" definition was adopted at the contact surface between purlins and roof sheets. For the sake of computational efficiency, the symmetry of the model was utilized, with only half of the structure being modeled. Symmetry constraints were imposed along the lengths of the roof sheets and lateral struts. The purlin was assumed to be pin-supported at both ends through four bolt holes, resembling cleat support. Constraints in the purlin length direction were set to prevent rigid motion. Concentrated loads were applied at corresponding positions on the sheets via reference points to imitate downward loading conditions. Mesh size of the model was applied as a 1 mm mesh length was assigned around screw holes and a 20 mm mesh length was utilized for other regions.

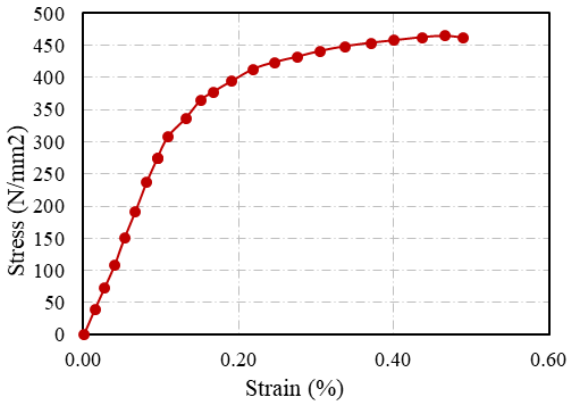

Figure 4. Stress vs. strain curves adopted in FEM

RESULTS DISCUSSION

The ultimate applied load (Pu) and critical bending moment (Mt) of four specimens are demonstrated in Table 2. Among thost specimens, Z30720 exhibits the highest failure load (70.31 kN) and bending moment capacity (17.31 kNm), while Z14614 demonstrates the lowest results (24.13 kN and 5.72 kNm). For Z14618 and Z14618, an increase in section thickness from 1.4 mm to 18 mm (a 28.6% increment) results in a 36.7% enhancement in Pu, indicating the influence of purlin section thickness on moment capacity. Furthermore, the overall behaviour of the purlin is significantly impacted by the depth of the purlin cross-section. With a 37.9% increase in section depth from Z14618 to Z20618, Pu improves by 44.5%.

Figure 5 shows curves of the applied load to deflection relationships obtained from experimental and numerical methods, demonstrating a strong agreement with a maximum discrepancy of 3.0%. As shown in Table 2, specimens with thinner gauges (less than 1.5 mm) predominantly failed in the LB+DB mode, while the majority of thicker specimens (t > 1.5 mm) exhibited failure in the DB mode. Figure 6a illustrates a combined buckling mode, such as LB on the web and DB on the top flange, observed in Z14614. Conversely, for the remaining specimens, DB buckling mode occurred at the top flange under the loading point (Figure 6b). Additionally, Figure 6c demonstrates DB occurring in both lateral struts.

Table 2. Comparison of load results

Specimen	P_u (kN)	M_t (kNm)	P_{FEM} (kN)	P_{FEM}/P_u	Failure mode
Z14614	24.13	5.72	22.15	0.97	LB+DB
Z14618	32.42	7.82	32.28	1.03	DB
Z20618	46.38	11.30	45.81	1.01	DB
Z30720	70.31	17.31	68.8	0.99	DB

Note: Lateral torsional buckling.

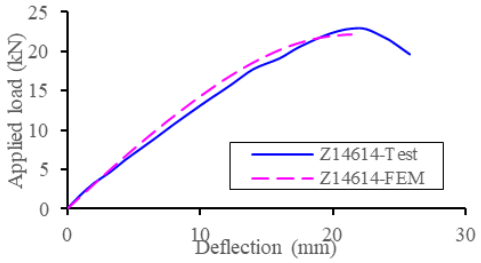

(a) Z14614

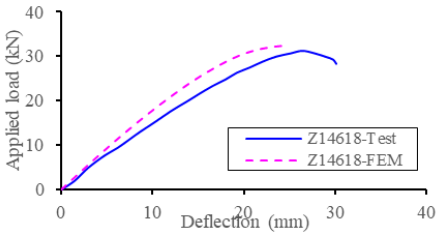

(b) Z14618

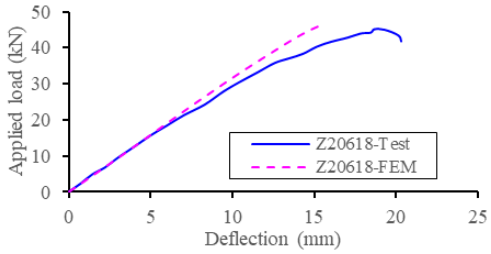

(c) Z20618

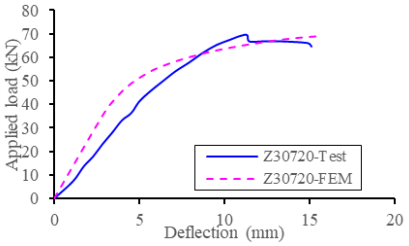

(d) Z30720

Figure 5. Comparison of load vs. deflection curves

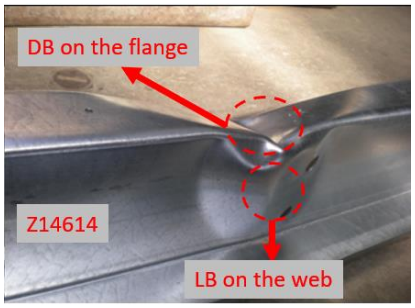

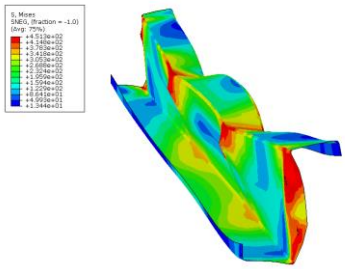

(a) LB and DB on the purlin

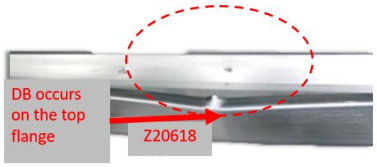

(b) DB on the purlin

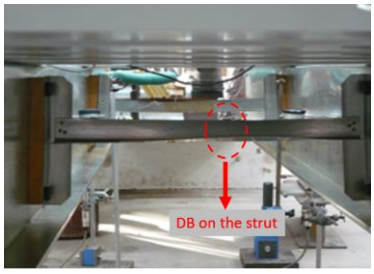

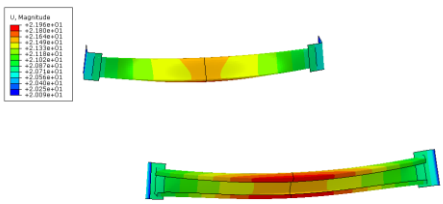

(c) DB on the strut

Figure 6. Comparison of typical failure behaviours

PARAMETRIC STUDIES

Figure 7 highlights the substantial impact of purlin thickness and yield strength on structural load-bearing capacity. For purlins with a height of 145 mm, increasing the thickness from 1.2 mm to 1.4 mm, 1.8 mm, and 2.0 mm results in applied load improvements of 34%, 97%, and 144%, respectively. Similarly, for 200 mm high purlins, raising the thickness from 1.4 mm to 1.6 mm, 1.8 mm, 2.0 mm, and 2.5 mm leads to respective capacity increases of 30%, 44%, 54%, and 73%.

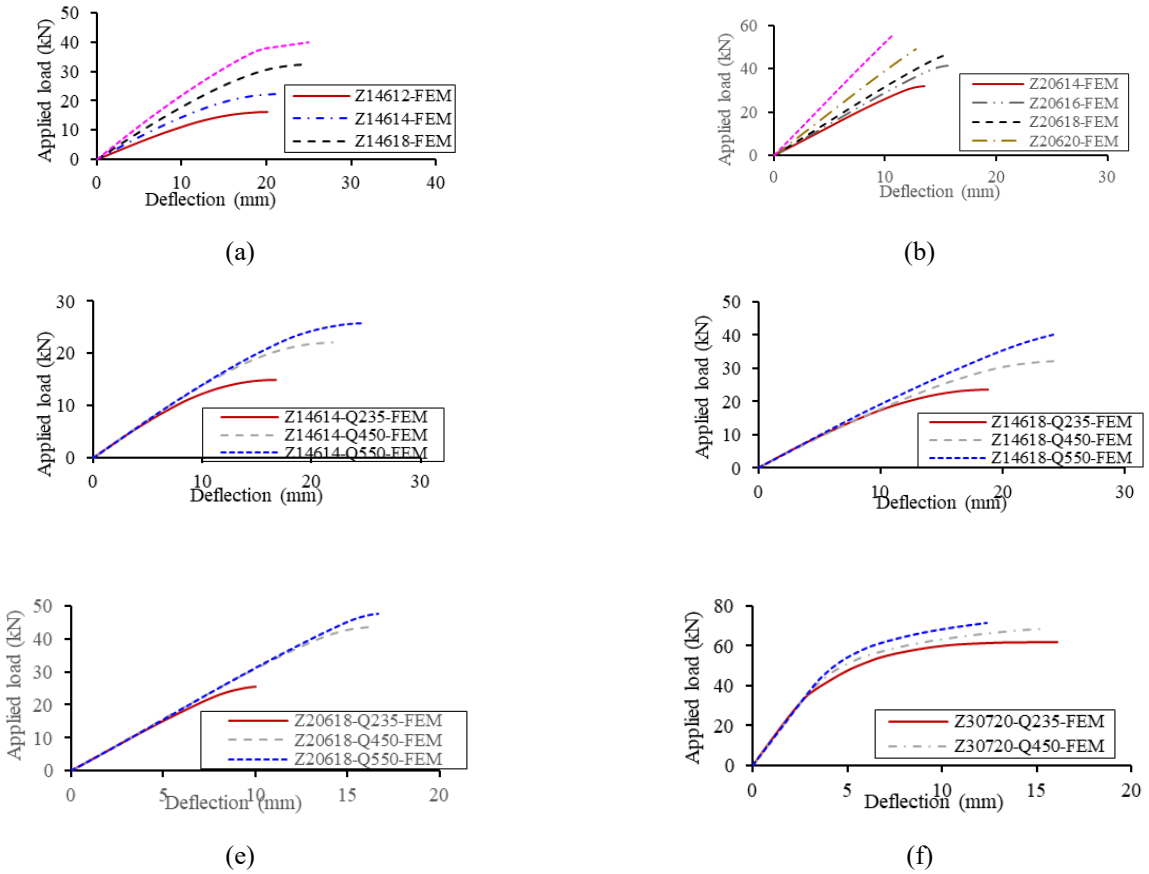

Figure 7. Effect of purlin thickness and purlin yield strength

The study also examined the structure's load-bearing capacity under three purlin strength levels: Q235 (yield strength of 235 MPa), Q450 (yield strength of 450 MPa), and Q550 (yield strength of 550 MPa). Increasing the yield strength from Q235 to Q450 resulted in a 91% strength improvement, leading to load-bearing capacity increases of 48%, 37%, 71%, and 11% for Z14614, Z14618, Z20618, and Z30720, respectively. Similarly, transitioning from Q450 to Q550 yielded a 22% strength increase, with corresponding capacity enhancements of 17%, 24%, 9%, and 3% for the same purlin models.

To assess the contribution of lateral constraints on the structural resistance, the study conducted a comparison under varying roof panel thicknesses tp and different quantities of lateral support struts (S0, S1 and S2 represent 0, 1 and 2 struts in the model). As shown in Figure 8, it reveals that because of the existence of lateral support struts, the influence of roof panel thickness on the structural load-carrying capacity is relatively minor. With an increase in thickness from 0.7 to 1.2, the change in load-bearing capacity remained below 3%. For Z14614, Z14618, Z20618, and Z30720, the introduction of additional lateral support struts resulted in notable increases in load-bearing capacity. Specifically, when transitioning from 0 to 1 lateral support strut, the load-bearing capacity increased by approximately 9%, 5%, 2%, and 18%, respectively. Similarly, an increase from 1 to 2 lateral support struts yielded load-bearing capacity increments of approximately 4%, 2%, 1%, and 2%, respectively. This phenomenon is attributed to the occurrence of LTB when purlins lack full lateral restraint, leading to twisting and sideways shifting under loading conditions (see Figure 9).

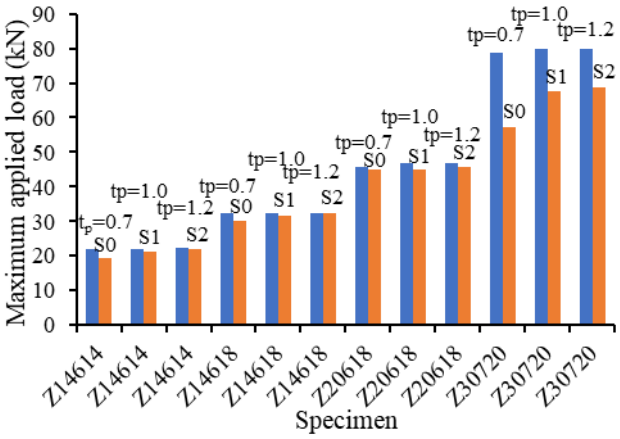

Figure 8. Effect of lateral struts and panel thickness

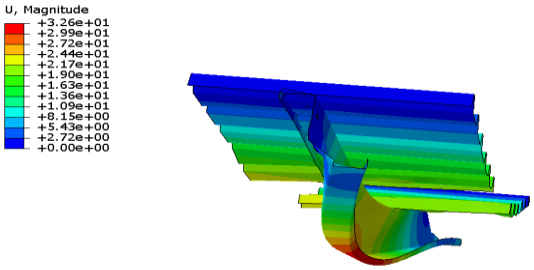

Figure 9. LTB occurs on the purlin-sheet system when lateral struts were not considered

CONCLUSIONS

This paper aims to evaluate the performance characteristics of CFS sheet-to-purlin systems, with particular emphasis on the effect of lateral support struts. The key findings are as follows:

The thickness of the purlins has a profound impact on the system's resistance, while the material strength of the purlins also plays a critical role. In contrast, the effect of roof panel thickness is relatively minor. This phenomenon arises from the presence of lateral support bars, which effectively prevent LTB in the purlins. The primary role of the roof panel lies in providing lateral restraint, thereby limiting its contribution to the overall system performance.

At lower purlin thicknesses, the dominant failure modes observed are DB at the top flange and LB at the web. As the thickness of the purlins increases, the predominant buckling mode gradually transitions towards DB. However, the removal of lateral support may lead to a shift in the buckling mode towards LTB.

ACKNOWLEDGEMENT

The authors express their thanks for the sponsor from the Science and Technology Project of State Grid Zhejiang Electric Power Co., Ltd. (SGZJQZ00JJJS2310864).

REFRENCES

[1] Bai, F., Yang, N., Wang, X., et al. 2021. Modified DSM framework for limit states prediction of simply-supported Z-section purlin with sheeting. Engineering Structures, 231, 111789.

[2] Pařenica, P., Rosmanit, M., Flodr, J. 2017. Numerical Modelling of Thin-walled Purlins Connection tothe Supporting Structure. Procedia Engineering, 190, 186-192.

[3] Pham, C. H., Davis, A. F., Emmett, B. R. 2014. Numerical investigation of cold-formed lapped Z purlins under combined bending and shear. Journal of Constructional Steel Research, 95, 116-125.

[4] Ling, J. Y., Kong, S. L., De'nan, F. 2015. Numerical study of buckling behaviour of cold-formed C-channel steel purlin with perforation. Procedia Engineering, 125, 1135-1141.

[5] Zhang, L., Tong, G. S. 2016. Lateral buckling of simply supported C- and Z-section purlins with top flange horizontally restrained. Thin-Walled Structures, 99, 155-167.

[6] Zhang, L., Tong, G. S. 2016. Lateral buckling of C-section purlins with one anti-sag bar at middle span section. Thin-Walled Structures, 102, 246-257.

[7] Ye, Z.-M., Kettle, R. and Li, L.-Y. 2004. Analysis of cold-formed zed-purlins partially restrained by steel sheeting. Computers & Structures, 82, 731-739.

[8] Ye, Z.-M., Kettle, R., Li, L.-Y., et al. 2002. Buckling behavior of cold-formed zed-purlins partially restrained by sheeting. Thin-Walled Structures, 40, 853-864.

[9] Eurocode 2006. Eurocode3: Design of Steel Structures: Part-1-3 General rules- Supplementary rules for cold-formed members and sheeting.

[10] Vran, T. 2002. Torsional restraint of cold-formed beams provided by corrugated sheeting for arbitrary input variables. Eurosteel the 3rd European conference on steel structures. Coimbra, Portugal.

[11] Zhao, C., Yang, J., Wang, F., et al. 2014. Rotational stiffness of cold-formed steel roof purlin–sheeting connections. Engineering Structures, 59, 284-297.

[12] Soroushian, P. and Peköz, T. 1981. Behavior of c- and z-purlins under wind uplift. The 6th International Specialty Conference on Cold-Formed Steel Structures, 1982.

[13] Basaglia, C., Camotim, D., Gonçalves, R., et al. 2013. GBT-based assessment of the buckling behaviour of cold-formed steel purlins restrained by sheeting. Thin-Walled Structures,72, 217-229.

[14] Georgescu, M., Ungureanu, V. 2014. Stabilisation of continuous Z-purlins by sandwich panels: Full scale experimental approach. Thin-Walled Structures, 81, 242-249.

[15] Michal Gajdzicki. 2018. Sheet-to-purlin fasteners arrangement and the value of rotational restraint of cold-formed Z-purlins. Journal of Constructional Steel Research, 151, 185-193.

[16] Kujawa, M., Szymczak, C. 2014. Numerical and experimental investigation of rotational stiffness of zed-purlins connection with sandwich panels. Thin-Walled Structures, 75, 43-52.

[17] Yang, J., Liu, Q. 2012. An experimental study into flexural behaviour of sigma purlins attached with roof sheets. Engineering Structures, 45, 481-495.